Turkish Computational and Theoretical Chemistry

Turkish Comp Theo Chem (TC&TC)

Volume(Issue): 7(2) – Year: 2023 – Pages: 34-57

e-ISSN: 2602-3237

https://doi.org/10.33435/tcandtc.1151841

Received: 31.07.2022 ***Accepted***: 08.12.2022 *Research Article*

Effects of flavonoids on SARS–CoV–2 main protease (6W63): A molecular docking study

Tugba Ertan-Bolelli[a,b], Kayhan Bolelli[a,b], Cisem Altunayar-Unsalan[c], Ozan Unsalan[d, 1], Berguzar Yilmaz[e]

[a]Ankara University, Faculty of Pharmacy, Department of Pharmaceutical Chemistry, 06560, Ankara, Turkey
[b]Bolelli Lab LLC, Stone Mountain, GA-30083, USA
[c]Ege University, Central Research Testing and Analysis Laboratory Research and Application Center, 35100, Bornova, Izmir, Turkey
[d]Ege University, Faculty of Science, Department of Physics, 35100, Bornova, Izmir, Turkey
[e]Department of Biotechnology, Graduate School of Natural and Applied Science, Ege University, Izmir, Turkey

Abstract: Public health is still under attack by a worldwide pandemic caused by a coronavirus which is known to cause mainly respiratory and enteric disease in humans. Currently, still limited knowledge exists on the exact action mechanism and biology of SARS–CoV–2 although there are several effective vaccines and antiviral treatment. Besides, there is a considerable amount of 3D protein structures for SARS–CoV–2, related to its main protease resolved by X–ray diffraction. Here, we used molecular docking strategy to predict possible inhibitory activities of flavonoids on SARS–CoV–2 Mpro enzyme. For this, 800 flavonoids were retrieved from the ZINC database. Results suggested that avicularin was the lead flavonoid which docked to Mpro with the best binding energy. However, most of flavonoids showed H–bond interactions with Hie–41 and Cys–145 catalytic dyad, which were important residues for the catalytic activity of SARS–CoV–2 Mpro. Strong hydrogen bonding (2.36 Å) with Sγ atom of Cys145 residue was observed. This might suggest an initial formation of covalent bonding. Findings showed that selected flavonoids could be promising inhibitors of this enzyme and have the potential for future therapeutic drugs against COVID–19 after immediate experimental validation and clinical approvals.

Keywords: COVID–19; SARS-CoV-2; Flavonoids; Molecular docking; catalytic dyad.

1. Introduction

Coronaviruses (CoVs) are known to cause mainly respiratory and enteric diseases in humans and animals [1]. They are mainly divided into four genera, alpha, beta, gamma and delta–CoV [2]. As of July 10, 2022, this virus which has already spread to almost all countries with 555,030,991 confirmed total cases and 6,350,601 global deaths [3]. Currently, limited knowledge exists on the exact action mechanism and biology of SARS–CoV–2 ("Severe Acute Respiratory Syndrome Corona Virus–2" as seventh member of beta group [4]) and there is a limited number of effective vaccines and antiviral treatment against it. Regarding the efforts to discover a more effective vaccine, there are numerous achievements globally which produced vaccines since November 2020, Pfizer Inc [5], Moderna [6] and the University of Oxford (in collaboration with AstraZeneca) [7,8] announced positive results from provisional analyses of their Phase III vaccine trials. However, according to Coalition for Epidemic Preparedness Innovations (CEPI) most of the platforms of vaccine candidates in clinical trials are focused on the coronavirus spike protein and its variants as the primary antigen of COVID–19 infection [9]. Based on the data from COVID19 Vaccine Tracker website, there are 38 approved vaccines [10]. A research reported that 76

[1] Corresponding Authors
e-mail: physicistozan@gmail.com

total vaccine candidates dominantly exist from protein subunit among other molecular platforms such as non-replicating viral (31) vector, RNA-based (31), replicating viral vector (21), DNA-based (19), inactivated virus (14), virus-like particle (13), and live attenuated virus (4) platforms [11]. On the other hand, there is a considerable amount of 3D protein structures for SARS–CoV-2, generally related to its main protease structure resolved by mostly X-ray diffraction crystallography, available in Protein Data Bank (RCSB PDB). Although, exact action mechanism/(s) of COVID–19 is still a mystery itself, it was reported that it has the same cell-entry receptor, ACE2 (Angiotensin-Converting Enzyme 2), for infection as SARS–CoV [12,13]. Like main protease and ACE2 structures, 3C-like Proteinase of COVID–19 was also successfully expressed [14,15]. Moreover, the number of infections is globally still rising [16] and immediate increase in the publication of over 10,000 peer-reviewed papers showed the importance and urgent need for discovery and development of effective and preventive therapeutic drugs/protocols and vaccines.

Traditional herbal medicines are known to be used and it was recently reported that these medicines have been used in China from the beginning of the outbreak and they were seen to recover of 90% of the 214 patients treated [17,18]. Some promising results were also published by Xu et al. in Zhejiang Province–China [19]. Chinese traditional medicines, Shu Feng Jie Du and Lianhuaqingwen, were recommended because of their efficiency against previous influenza A (H1N1) or SARS–CoV–1 [20]. According to a recent investigation, researchers from the Zhongnan Hospital of Wuhan University recommended traditional Chinese medicines in the guidelines for the treatment and prevention of COVID–19 to treat the disease by using different herbal mixtures according to the disease-stage [21]. Flavonoids are a large class of naturally occurring phenolic compounds distributed in the plant kingdom. Almost more than 4,000 varieties of flavonoids have been previously identified. These broad-spectrum compounds act as potent antioxidants, and display antiallergic, anti-inflammatory, antimutagenic, antihemorrhagic, antineoplastic, and hepatoprotective activities [22,23]. They also exhibit biological activities including anticancer, antibacterial, antifungal, and antiviral activities. Among flavonoids, apigenin, luteolin, and quercetin were shown to possess antiviral activities both in-vivo and in-vitro [24,25]. Several natural compounds including baicalin, scutellarin, hesperetin, nicotianamine and glycyrrhizin were predicted to have capacity for binding ACE2 receptor with potential anti-2019–nCoV effects [25]. Moreover, quercetin, daidzein, puerarin, epigallocatechin, epigallocatechin gallate, gallocatechin gallate and kaempferol were reported to inhibit the proteolytic activity of SARS–CoV 3CLpro [26,27]. Among flavonoids, quercetin, quercetin derivatives, catechin, epicatechin, epicatechin gallate and epigallocatechin gallate were reported to inhibit Lpro SARS–3C expressed in Escherichia coli [28–30]. Usage of flavonoids that exist in many herbal plants can be evaluated as an alternative approach to chemically synthesized therapeutic drugs against many viruses including CoVs. In addition, chemical structures and vibrational spectroscopic properties of flavonoids such as baicalein, naringenin, and selected amino-, chloro-, and bromo-flavones were previously investigated in detail [31–36] and they have also been investigated against a wide range of DNA and RNA viruses [37]. For example, apigenin is active against picornavirus (RNA virus), inhibiting protein synthesis by suppressing internal ribosome entry site (IRES) viral activity [38]. Epigallocatechin-3-gallate (EGCG), active polyphenolic catechin that accounts for approximately 59% of the total catechins from the leaves of the green tea (Camellia sinensis (L.), Kuntze) interferes with the replication cycle of DNA viruses, such as hepatitis B virus, herpes simplex, and adenovirus [39].

It is quite useful and efficient to apply computer-aided drug design and molecular docking techniques to quickly identify promising candidates against diseases, especially after detailed 3D-structures of various key proteins of that disease are resolved experimentally. Although there are efforts appeared currently, there is still a lack of docking studies performed with especially flavonoids on different main proteases of SARS–CoV–2. The importance of Mpro in the life cycle of SARS–CoV–2 identifies the Mpro as an attractive target for antiviral drug design. SARS–CoV–2 Mpro (6LU7) was docked with fourteen flavonoid compounds as well as four already existing drugs and the binding energies were determined [40]. We used 6W63 for our non-covalent docking, as its natural ligand (X77) is non-covalent whereas 6LU7 ligands are covalent. Taking the advantage of a recently deposited crystal structure of SARS–CoV–2 Mpro (6W63) in complex with its natural inhibitor [41], we used virtual screening approach and found that three FDA approved drugs can be used against inhibition of Mpro of SARS–CoV–2 [42]. Virtual screening research already was shown be able to replace time-consuming efforts in determination of new targets for the existing drug compounds as demonstrated in earlier articles including SARS–CoV–2 [43–63]. In addition, some recent investigations on flavonoids showed and discussed the high potential of flavonoids docked to MPro of SARS–CoV–2 [64–70]. In addition, our previous virtual screening study [42] showed that two FDA approved drugs, fenoterol and dobutamine, can be considered as promising inhibitors for SARS–CoV–2 Mpro. Moreover, regarding 113 FDA approved drugs in clinical trials for COVID–19 treatment, it has been identified activated signaling pathways associated with the infection caused SARS–CoV–2 in human lung epithelial cells through integrative analysis. Then, the activated gene ontologies (GOs) and top lead super GOs were identified [71] and fenoterol was among these GOs. Their findings appear to support our conclusions on fenoterol and dobutamine [42].

The objectives of this study were: i) to determine important active site amino acids by structure-based sequence alignment of SARS–CoV–2 Mpro ii) to identify potential non-covalent Mpro inhibitors by screening protease-inhibitor-like compounds, particularly flavonoids as candidates, which are available in the ZINC database by molecular docking studies iii) to validate the stable binding of the lead compounds with SARS–CoV–2Mpro (6W63) and iv) to calculate binding affinities (kcal/mol) for each lead compound.

2. Computational Method

Molecular docking procedures are used for the purpose of selecting the hits that exhibit chemical, structural, and electronic characteristics. The information of the target protein can be derived from in silico technique or experimental data. In order to predict the possible inhibitory activities of flavonoids, we performed docking studies on SARS–CoV–2 Mpro enzyme using Schrödinger 2019-4 software, with Maestro 12.2 and the Glide 8.5 module to predict the binding energies [39,72,73].

2.1. Protein preparation

X-ray crystallographic structure of SARS–CoV–2 Mpro was retrieved from Protein Data Bank (6W63) and prepared for docking process. This enzyme have 306 residues and resolution of the structure is 2.10Å [74]. In order to prepare the enzyme, we used the protein preparation wizard module. During preparation hydrogen atoms were added and bond orders were assigned with zero order bonds to disulfide bonds and metals as well. Water molecules were removed within 3 Å of het groups. OPLS-2005 force field for minimization and pH =7.0 ± 2.0 were chosen to minimization step.

2.2. Ligand preparation

Approximately 800 flavonoids were retrieved from the ZINC [75] database to perform the molecular docking studies and prepared by using Schrödinger, LigPrep module [76]. Flavonoids were prepared and 3D structures were generated by adding hydrogen atoms and removing salt. The bond angles and bond orders were assigned after ligand minimization step. In order to keep the ligands in the right protonation state in biological conditions, Epik option was used. LigPrep can generate the expected ionized forms at significant concentrations corresponding to the pH 7.0±2.0, generate variations, perform verification, and optimize structures. It generates a maximum of 32 stereochemical structures per ligand.

2.3. Grid Generation

The active site of SARS–CoV–2 Mpro was defined for generating the grid in Maestro. The grid box was limited to the size of 10 Å in –20.46, 18.11, and –26.91 directions at the active site. First, docking procedure was validated by extracting the nature ligand, X77 from the binding site and re-docking it to SARS–CoV–2 Mpro by using the Glide SP (standard precision glide docking) module [77]. Glide generates conformations internally and passes these through a series of filters. Glide successfully reproduced the experimental binding conformations of X77 in SARS–CoV–2 MPro with an acceptable root-mean-square deviation (RMSD) value of 0.68 Å. Then, flavonoids were screened by using the same grid with Glide XP (Extra precision glide docking) module [73]. According to the docking scores 16 hit flavonoids were selected.

2.4. DFT computation

In addition, geometric structure of the top hit compound, avicularin, was optimized by Gaussian 09 software by using DFT method with B3LYP functional by 6-311++G(d,p) basis set. Vibrational wavenumbers were scaled with 0.967 and 0.955 for the wavenumbers below and above 1800 cm□1, respectively.

3. Results and discussion

In this study, we used molecular docking strategies to predict the possible inhibitory activities of some flavonoids on SARS–CoV–2 Mpro enzyme. For this purpose, approximately 800 flavonoids were retrieved from the ZINC database. According to docking results, we selected 16 hit flavonoids and the docking scores and the interactions were shown in Table 1 together with the data for natural ligand, X77. Structures of these top 16 flavonoids were given in Figure 1. Binding modes of the selected flavonoids on SARS–CoV–2 Mpro (6W63) and their interactions with the surrounding residues in two-dimension representation were given in Figure 2. Compound 469 (Avicularin) and 471 showed the best two docking scores as –11.799 and –10.789, respectively. As presented in Table 1, avicularin showed H-bonds with Gly143, Hie163, and water mediated H-bonds with Hie41 and Glu166 whereas the compound 471 showed H-bonds with Gly143, Cys145, Hie163, water mediated H-bond with Glu166 and π-π stacking with Hie41 (Figure 2). Although avicularin has the best docking score, we presented compound 471 in Figure 3 because it is the most interacting compound with its environment. It is interesting to note that both compounds (avicularin and 471) have the same flavonoid skeleton with the four (two in B ring and two in A ring) identically located OH groups in their molecular structure but act differently for the inhibition of 6W63. Furan rings are above and below the skeleton for 471 and avicularin, respectively. OH groups are consecutively located in both compounds. For 471, OH groups are in up-up-down fashion whereas OH groups of avicularin in down-up-down fashion. The interaction type and the number of the interactions with the surrounding residues is strongly affected by these orientations of these groups. Binding mode of compound 471 with SARS–CoV–2 Mpro (6W63) together with the catalytic center was shown in Figure 3. Most of the selected flavonoids showed H-bond interactions with Hie41 and/or Cys145 [78–80], which were important residues for the catalytic activity of SARS–CoV–2 Mpro with the better docking scores than the natural ligand X77. Avicularin was recently shown to have docking capabilities with different interaction sites of various main proteases such as, 6W4B, 6VYB, 6LVN, 6M0J, and 6LU7 and it showed no toxicity and undesired effects like tumorigenicity, mutagenicity, irritating, or reproductive effects [65].

Distances between the active site residues of Mpro on interaction with the selected flavonoids were presented in Table 2. From our findings, it is evident that the distances between Cys145 and the investigated compounds are found to be between 2.30 (compound 471) and 4.0 Å (compounds 425 and 424). Regarding Hie41, these data fell into the region between 2.57 (compound 454) and 5.66 Å (compound 468). Aside from Cys-Hie residues, Gly143 revealed closer distances when compared to Cys-Hie residues. For example, we observed strong hydrogen bonding with Gly143 (with 1.65 Å distance) for compound 435. The structure of the 6W63 complex at 2.10 Å resolution [41] is well enough for us to distinguish the hydrogen bonds given in Table 2. In addition, although the thiol group of Cys145 interacts to the compound 471 with a bond of 2.30 Å, it was confirmed that the main chains of Gly143, Hie163, and Glu166 also interact with each inhibitor mostly. In addition, it is interesting to note that we could observe the Pi-stacking formation only between imidazole ring of Hie41 and the ligand 420. This ligand was also seen to be interaction via Sγ atom of the Cys145. According to the results of Yoshino et al. (2020), hydrogen bond donor pharmacophore sphere is located near Hie41. Their results suggested that any hydrogen bond acceptor functional group could have the potential to contact with Hie41. As depicted in Figure 5, our results are in agreement with their work [81] and we could identify both strong hydrogen bonding (2.36 Å) with Sγ atom of the Cys145 and Pi-stacking formation between the imidazole ring of Hie41 and phenyl ring of compound 420. Moreover, the water bridges constructed among the residues and the ligands also contribute to Mpro and inhibitor complex structure to stabilize the structure, functional groups of ligands.

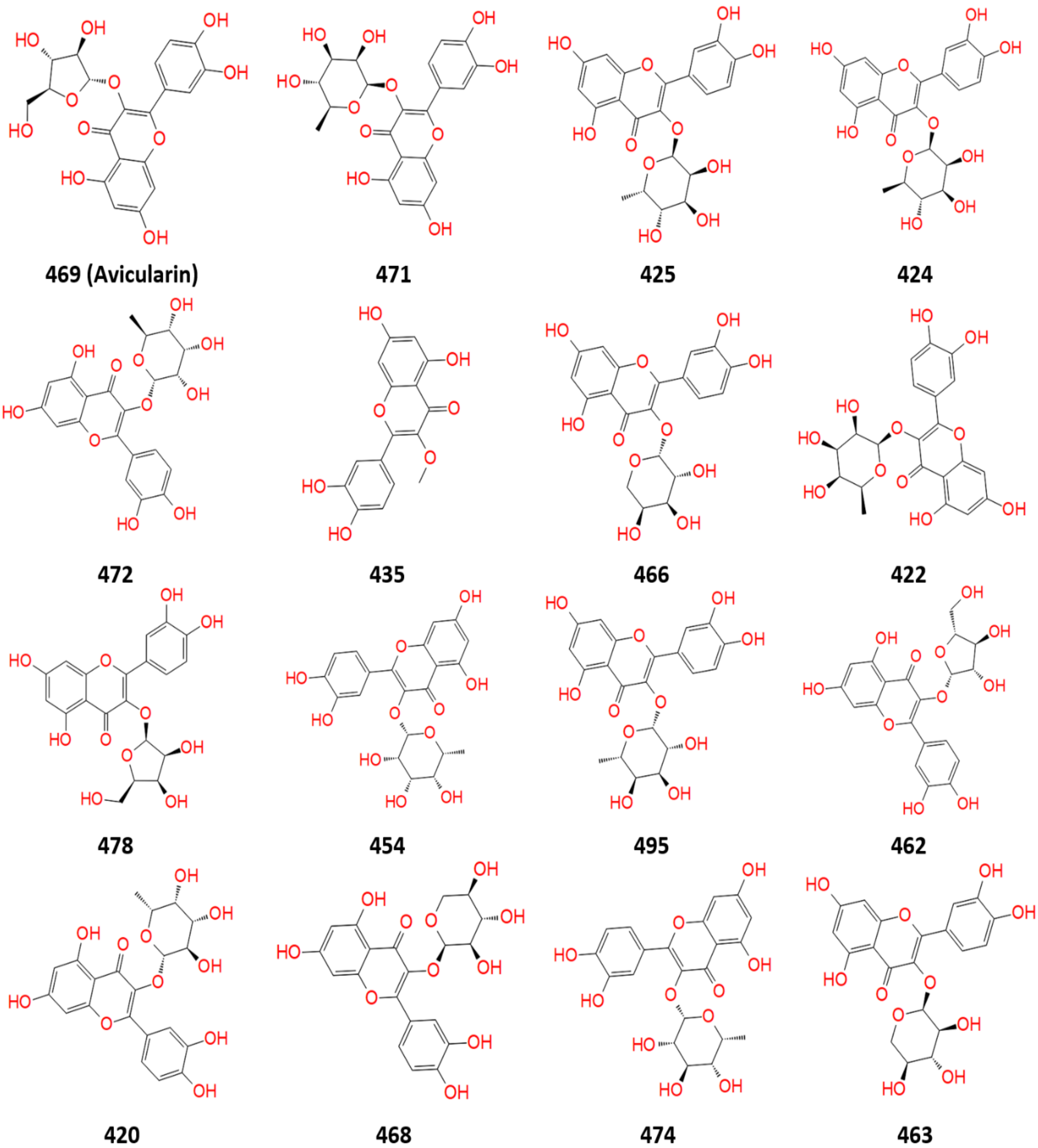

Figure 1 Molecular structures of the 16 hit flavonoids with the top lead Avicularin (#**469**).

Table 1. Docking results of the 16 hit flavonoids.

Compound	ZINC ID	Docking Score (kcal/mol)	Glide Score (kcal/mol)	Interactions
469 (Avicularin)	ZINC28540146	–11.799	–11.828	Thr25[d], Thr26[d], Leu27[c], **Hie41 (water mediated)**[d], Phe140[c], Leu141[c], Asn142[d], **Gly143**[f], Ser144[d], Cys145[c], **Hie163**[d], His164[d], Met165[c], **Glu166 (water mediated)**[a], Pro168[c], Arg188[b], Gln189[d], Thr190[d], Gln192[d], **H_2O**
471	ZINC33833455	–10.789	–10.817	Thr25[d], Thr26[d], Leu27[c], Hie41[d,e], Met49[c], Phe140[c], Leu141[c], Asn142[d], **Gly143**[f], Ser144[d],

				Cys145[c], **Hie163**[d], His164[d], Met165[c], **Glu166 (water mediated)**[a], Asp187[a], Arg188[b], Gln189[d], Thr190[d], Gln192[d], **H_2O**
425	ZINC4416344	–10.467	–10.496	**Hie41 (water mediated)**[d], Cys44[c], Met49[c], Tyr54[c], Phe140[c], **Leu141(2)**[c], Asn142[d], **Gly143**[f], Ser144[d], **Cys145**[c], **Hie163**[d], His164[d], Met165[c], **Glu166 (water mediated)**[a], Pro168[c], Hie172[d], Asp187[a], Arg188[b], Gln189[d], Thr190[d], Gln192[d]
424	ZINC4416342	–10.167	–10.195	Thr25[d], Hie41[d], Cys44[c], Met49[c], Pro52[c], Tyr54[c], Tyr118[c], Phe140[c], L**eu141(2)**[c], Asn142[d], Gly143[f], Ser144[d], **Cys145**[c], **Hie163**[d], His164[d], Met165[c], Glu166[a], Pro168[c], Hie172[d], Asp187[a], Arg188[b], Gln189[d]
472	ZINC33833712	–9.968	–9.997	Hie41[d], **Cys44**[c], Met49[c], Pro52[c], Tyr54[c], Leu141[c], Asn142[d], **Gly143**[f], Ser144[d], Cys145[c], Met165[c], **Glu166 (water mediated)**[a], Leu167[c], Pro168[c], **Asp187**[a], Arg188[b], Gln189[d], Gln192[d]
435 (3-O-Methylquercetin)	ZINC5998596	–9.837	–9.871	Hie41[d], **Cys44**[c], Met49[c], Pro52[c], Tyr54[c], Leu141[c], Asn142[d], **Gly143**[f], Ser144[d], Cys145[c], Met165[c], **Glu166**[a], Asp187[a], Arg188[b], Gln189[d], **H_2O**
466	ZINC15657718	–9.652	–9.681	Hie41[d], Cys44[c], Met49[c], Phe140[c], **Leu141(2)**[c], Asn142[d], **Gly143**[f], Ser144[d], Cys145[c], **Hie163**[d], His164[d], Met165[c], Glu166[a], Pro168[c], Asp187[a], Arg188[b], Gln189[d]
422	ZINC4416338	–9.627	–9.655	Thr25[d], **Hie41 (water mediated)**[d], Cys44[c], Met49[c], Pro52[c], Tyr54[c], Phe140[c], **Leu141**[c], Asn142[d], **Gly143**[f], Ser144[d], Cys145[c], **Hie163**[d], Met165[c], Glu166[a], Pro168[c], Hie172[d], Asp187[a], Arg188[b], Gln189[d]
478	ZINC61948742	–9.547	–9.575	Hie41[d], Cys44[c], Met49[c], Pro52[c], Tyr54[c], Leu141[c], Asn142[d], **Gly143**[f], Ser144[d], Cys145[c], Met165[c], **Glu166 (water mediated)**[a], Pro168[c], **Asp187**[a], Arg188[b], Gln189[d], Thr190[d], Gln192[d]
454	ZINC9147119	–9.502	–9.531	Hie41[d], **Cys44**[c], Met49[c], Pro52[c], Tyr54[c], Phe140[c], **Leu141**[c], Asn142[d], **Gly143**[f], Ser144[d], Cys145[c], **Hie163**[d], His164[d], Met165[c], **Glu166**[a], Pro168[c], Phe181[c], Asp187[a], Arg188[b], Gln189[d], Thr190[d], Gln192[d]
495	ZINC104891686	–9.345	–9.374	**Hie41 (water mediated)**[d], Cys44[c], Met49[c], Tyr118[c], Phe140[c], **Leu141(2)**[c], Asn142[d], **Gly143**[f], Ser144[d], Cys145[c], **Hie163**[d], His164[d], Met165[c], Glu166[a], Pro168[c], Arg188[b], Gln189[d]
462	ZINC14684606	–9.310	–9.339	Thr25[d], Thr26[d], Leu27[c], Hie41[d], **Cys44**[c], Met49[c], Pro52[c], Tyr54[c], Asn142[d], Gly143[f], Ser144[d], Cys145[c], Hie163[d], Met165[c], **Glu166**[a], Pro168[c], Asp187[a], Arg188[b], Gln189[d], **H_2O**
420	ZINC4349611	–9.205	–9.234	Thr25[d], Hie41[d,e], **Cys44**[c], Met49[c], Pro52[c], Tyr54[c], Leu141[c], Asn142[d], Gly143[f], Ser144[d], **Cys145**[c], His164[d], Met165[c], **Glu166**[a], Leu167[c], Pro168[c], Asp187[a], Arg188[b], Gln189[d], Thr190[d]
468	ZINC25763686	–9.172	–9.201	Thr25[d], Hie41[d], **Cys44**[c], Met49[c], Pro52[c], Tyr54[c], **Asn142**[d], Gly143[f], **Cys145**[c], Met165[c], **Glu166**[a], Pro168[c], **Asp187**[a], Arg188[b], Gln189[d], Thr190[d]
474	ZINC43465464	–9.150	–9.178	Hie41[d], Cys44[c], Met49[c], Tyr54[c], Phe140[c], **Leu141**[c], Asn142[d], **Gly143**[f], Ser144[d], Cys145[c], **Hie163**[d], His164[d], Met165[c], **Glu166**[a], Pro168[c],

				Hie172[d], Asp187[a], Arg188[b], Gln189[d], Thr190[d], Gln192[d]
463	ZINC14684625	–9.062	–9.091	**Hie41 (water mediated)**[d], Cys44[c], Met49[c], Tyr54[c], Phe140[c], **Leu141**[c], Asn142[d], **Gly143**[f], Ser144[d], Cys145[c], **Hie163**[d], His164[d], Met165[c], Glu166[a], Leu167[c], Pro168[c], Hie172[d], Asp187[a], Arg188[b], Gln189[d]
X77 (natural ligand)		−8.938	−8.938	Thr25[d], Thr26[d], Leu27[c], Hie41[d,e], Cys44[c], Met49[c], Pro52[c], Tyr54[c], Phe140[c], Leu141[c], Asn142[d,w], **Gly143**[f], Ser144[d], Cys145[c], **Hie163**[d], His164[d], Met165[c], **Glu166**[a], Leu167[c], Pro168[c], Hie172[d], Asp187[a], Arg188[b], Gln189[d]

Bold: H-bond, [a]negative charge (orange), [b]positive charge (cyan), [c]Hydrophobic (green), [d]Polar (turquoise), [e]π-π stacking, [f]glycine. Colors in this table refer to the colors given in Figure 2.

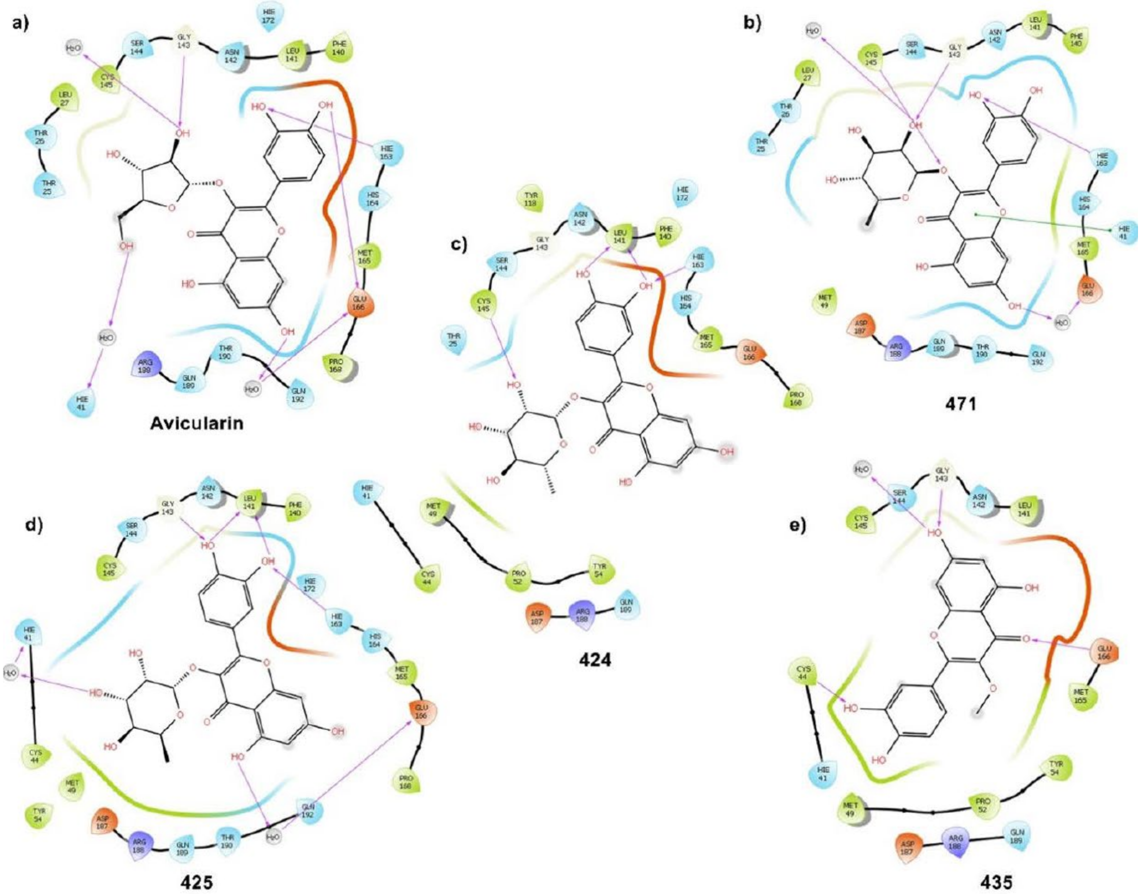

Figure 2 Binding modes of the selected lead flavonoids on SARS–CoV–2 M^{pro} (6W63) and their interactions with the surrounding residues.

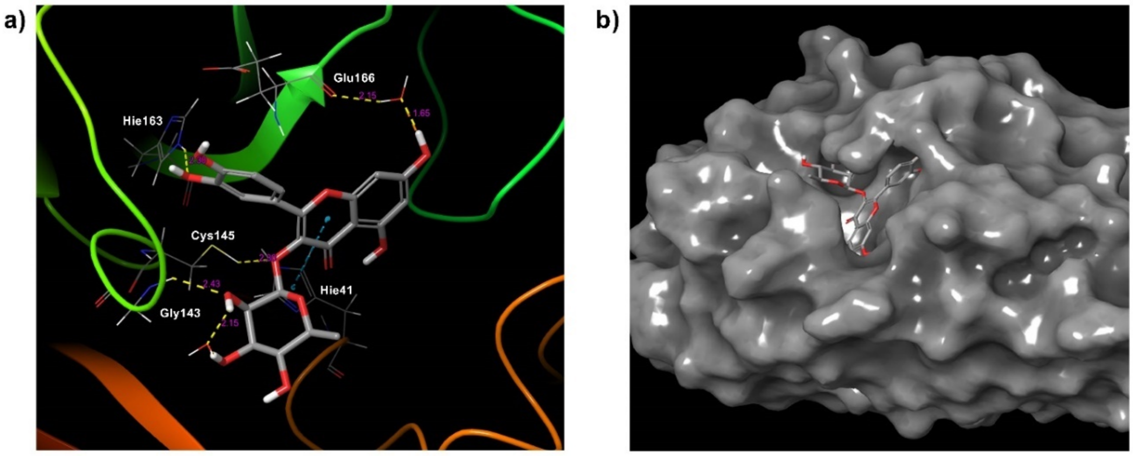

Figure 3 a) Binding mode of compound **471** with SARS–CoV–2 M^{pro} (6W63) together with the catalytic center shown as magnified view. The residues that participate in ligand are shown as stick models. Ligand is shown as ball-and-stick model. Strands represent the SARS–CoV–2 M^{pro} polypeptide with the side chain of Cys145 protruding. **b)** Ligand **471** in the binding pocket.

Table 2. Distances (Å) between the active site residues (Hie41, Gly143, Cys145) of M^{pro} on interaction with the selected flavonoids.

Compound	Hie41	Gly143	Cys145
420	5.41^{e}	2.24	**2.36**
422	**3.69 (water mediated)**	**2.15**	4.00
424	4.12	2.14	4.00
425	**4.12 (water mediated)**	**2.14**	4.00
435	4.78	**1.65**	3.90
454	2.57	**1.97**	3.27
462	5.01	2.01	3.55
463	**3.32 (water mediated)**	**2.12**	3.98
466	4.04	**2.04**	3.98
468	5.66	4.23	**2.36**
469	**3.41 (water mediated)**	**1.93**	2.41
471	5.43^{e}	**2.43**	**2.30**
472	4.82	**1.91**	3.43
474	2.67	**1.94**	3.35
478	4.87	**1.93**	2.41
495	**3.33 (water mediated)**	**2.10**	3.98

Bold: H-bond, **e:** π-π stacking (ring to ring distance was measured).

A recent investigation on the identification of key interactions between SARS–CoV–2 and various inhibitor drug candidates focused on the structures of three proteins, 6LU7, 2A5I, and 2OP9 took the advantage of molecular dynamics simulations and they suggested that the probability of the interaction of the amino acid residues for drug candidate indinavir was higher for Gly143 (54%) than their corresponding probabilities of natural ligands (30 and 36% for 2A51, and 2OP9) [81]. On the other hand, it is known that there are differences between protein structures, as 6W63 in our study, and binding profiles and interactions are quite different than each other. Consequently, this would lead difference interactions of drug candidates and their surrounding residues. We found that Gly143 is an important residue since our flavonoids are mostly in close contact with this residue.

The Mpro helps in replication and transcription of novel coronavirus and SARS–CoV–2 Mpro has a Cys-His catalytic dyad, and the substrate-binding site is in a cleft between domain I and domain II. These features are similar to previously reported Mpro from other coronaviruses [78–80]. It is widely accepted that increased inhibitor potency is related to the covalent bond formed between the active site residue and the designed compound. It was previously reported that the Sγ atom of Cys145 forms a covalent bond with the substrate, confirming that the Michael addition, has occurred

[82]. In contrast to that work, we were not able to detect any signal of Michael addition mechanism for none of our lead flavonoids, but this does not mean that such mechanism would not occur in the case of flavonoids. It is obvious that there are rapidly increasing numbers of MPro structures for this disease, and this would need more systematic research including molecular dynamics and experimental studies. However, our docking investigation revealed that almost all the selected flavonoids showed interactions with Hie41 and/or Cys145, with the better docking scores than the natural ligand X77. Even though numerous works emphasize Cys-His catalytic dyad residues Cys145 and Hie41, still there are a limited number of studies on Cys-His-Gly catalytic triad even this is a more complex mechanism compared to catalytic dyad. Furthermore, very rare Cys-His-Gly type of catalytic triad examples were previously be reported [83–85]. Even though the short distance (1.65 Å) between the Gly-143 and compound 435 might indicate a very strong hydrogen bond, this can be also attributed to an initial formation of a covalent bond. Of course, we are aware that it is still difficult to suggest or comment on this quickly, because occurring mechanisms of both catalytic dyads and triads are still not clear. Furthermore, regarding non-covalent inhibition aspects of compounds on main proteases, including flavonoids, appeared in recent publications demonstrated that it is rarely possible to design/discover non-covalent inhibitors, such as ML188 for SARS-CoV-1 Mpro which was shown to exhibit inhibition effects experimentally [86]. In that study, authors characterized the complex of SARS-CoV-2 Mpro with the non-covalent inhibitor ML188 and showed that ML188 has enhanced binding potency to SARS-CoV-2 compared to SARS-CoV-1. In addition, a recent X-Ray screening investigation identified active site and allosteric inhibitors of SRAS-CoV-2 Mpro. Researchers successfully found two allosteric binding sites from the yield of 37 compounds that bind to Mpro. A noncovalent binder MUT056399 (4-(4-ethyl-5-fluoro-2-hydroxyphenoxy)-3-fluorobenzamide) was also shown to block the active site of Mpro [87]. Even these rare compounds were encountered related to noncovalent bonding in terms of their inhibition effects experimentally, we must admit that experimental noncovalent binding profiles and inhibition effects of flavonoids particularly are still not crystal clear.

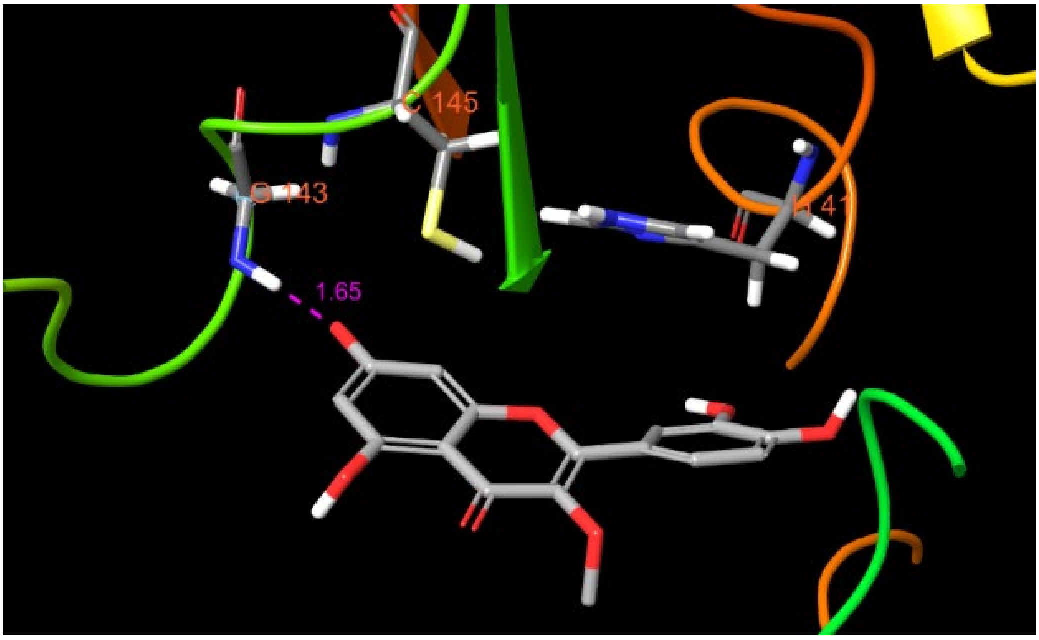

Figure 4 Compound **435** with its surrounding environment (Cys145-Hie41-Gly143).

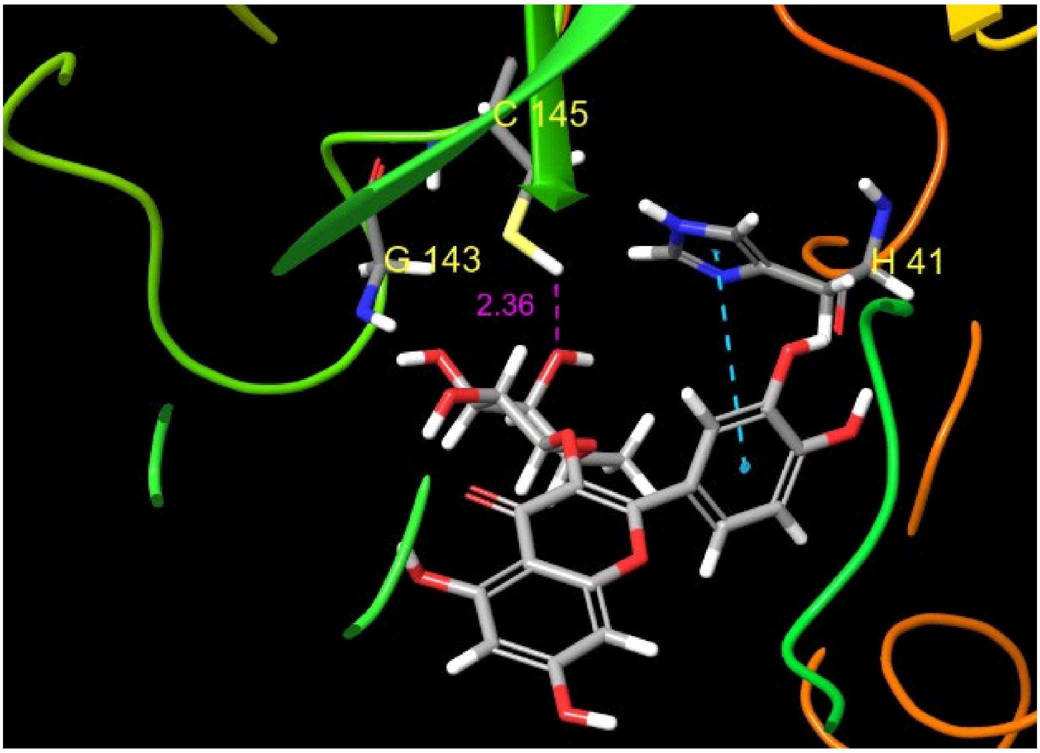

Figure 5 Stick diagram depicting the geometry and atomic interactions of the oxygen atom of compound **420** in H-bond linkage between the S_{γ} atom of Cys145. Light blue color denotes the π-π stacking between the phenyl ring of compound **420** and the Hie41.

Quantum chemical computations were performed on the top hit compound, avicularin, and optimized geometric structure was shown in Figure 6 together with the optimized parameters and vibrational wavenumbers (Table 3 and 4, respectively). Computed and scaled IR spectrum of avicularin was also given in Figure 7.

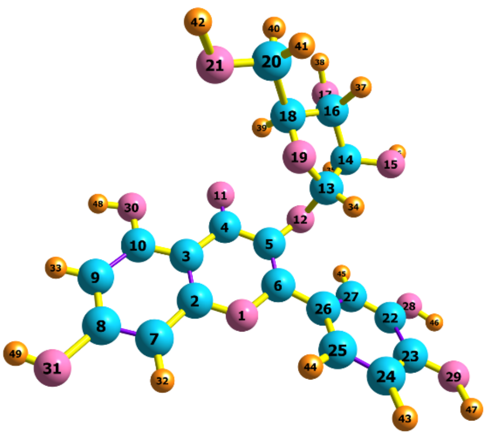

Figure 6. Optimized geometric structure of avicularin.

Optimized geometric structure of avicularin revealed that the twisted dihedral angle between the plane where A and C rings locate and the ring B was computed to be □29.94° which confirmed previously reported dihedral angle of several flavonoid analogs [35,88–91] that vary between ~18 to 21° with the exception of the group attached to C-ring's via its hydrogen atom (H12 in Figure 6). Due to the difference of the basic flavone structure (A-C-B structure), this value of dihedral angle would still be acceptable and this can be explained by weak interaction of the group between the B-ring of avicularin, thus this bending would take place.

C-H stretching, in-plane and out of plane CH bending modes were previously reported to be observed between 3100–3000, 1100–1500, and 800–1000 cm−1, respectively [92,93]. Our findings for avicularin were computed between 3079–2946 cm−1, 1104–1446 cm−1 799–905 cm−1 respectively and there is a good agreement with Varsanyi and Mohan's work [92,93]. O-H stretching vibrations were computed between 3675 and 3624 cm−1 whereas the peak that was observed at 1655 cm−1 was assigned to C=O stretching vibration and this assignment is in line with Heneczkowski and co-workers' previous work [94] where this band was assigned between 1649 and 1652 cm−1 for selected flavonoids in that study.

C=C stretching vibration were determined between 1606 and 1563 cm−1 while the bands computed between 1488 and 1480 cm−1 were attributed to CC stretching vibration of avicularin. In addition, CO stretching vibration was assigned between 1067 and 993 cm−1. Out-of-plane bending vibrations of avicularin were also computed below 904 cm−1 where these vibrations were previously emphasized to be observed in the same region [95].

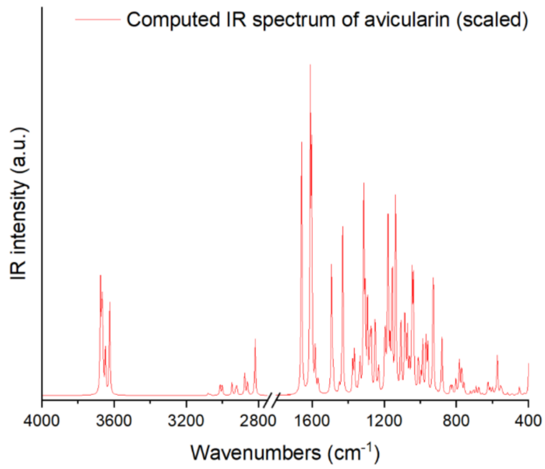

Figure 7. Computed (scaled) IR spectrum of avicularin.

Table 3. Optimized geometric structure of avicularin*.					
R(1,2)	1.363	A(2,1,6)	121.67	D(6,1,2,3)	2.18
R(1,6)	1.370	A(1,2,3)	121.59	D(6,1,2,7)	–178.51
R(2,3)	1.405	A(1,2,7)	114.70	D(2,1,6,5)	0.96
R(2,7)	1.393	A(3,2,7)	123.70	D(2,1,6,26)	–179.78
R(3,4)	1.477	A(2,3,4)	119.45	D(1,2,3,4)	–1.84
R(3,10)	1.419	A(2,3,10)	116.40	D(1,2,3,10)	179.10
R(4,5)	1.478	A(4,3,10)	124.13	D(7,2,3,4)	178.92
R(4,11)	1.222	A(3,4,5)	114.11	D(7,2,3,10)	–0.14
R(5,6)	1.357	A(3,4,11)	124.85	D(1,2,7,8)	–179.40
R(5,12)	1.372	A(5,4,11)	121.04	D(1,2,7,32)	0.28
R(6,26)	1.474	A(4,5,6)	122.49	D(3,2,7,8)	–0.11
R(7,8)	1.385	A(4,5,12)	115.83	D(3,2,7,32)	179.57
R(7,32)	1.081	A(6,5,12)	121.57	D(2,3,4,5)	–1.28
R(8,9)	1.400	A(1,6,5)	120.51	D(2,3,4,11)	178.49
R(8,31)	1.364	A(1,6,26)	111.37	D(10,3,4,5)	177.70
R(9,10)	1.392	A(5,6,26)	128.11	D(10,3,4,11)	–2.53
R(9,33)	1.087	A(2,7,8)	118.07	D(2,3,10,9)	0.32
R(10,30)	1.352	A(2,7,32)	120.70	D(2,3,10,30)	–179.80
R(12,13)	1.442	A(8,7,32)	121.23	D(4,3,10,9)	–178.69
R(13,14)	1.536	A(7,8,9)	120.72	D(4,3,10,30)	1.19
R(13,19)	1.402	A(7,8,31)	117.40	D(3,4,5,6)	4.39
R(13,34)	1.092	A(9,8,31)	121.89	D(3,4,5,12)	–179.38
R(14,15)	1.422	A(8,9,10)	120.37	D(11,4,5,6)	–175.39
R(14,16)	1.533	A(8,9,33)	120.05	D(11,4,5,12)	0.84
R(14,35)	1.094	A(10,9,33)	119.58	D(4,5,6,1)	–4.37
R(15,36)	0.962	A(3,10,9)	120.73	D(4,5,6,26)	176.50
R(16,17)	1.422	A(3,10,30)	118.46	D(12,5,6,1)	179.62
R(16,18)	1.539	A(9,10,30)	120.81	D(12,5,6,26)	0.49
R(16,37)	1.099	A(5,12,13)	116.62	D(4,5,12,13)	98.27
R(17,38)	0.962	A(12,13,14)	106.53	D(6,5,12,13)	–85.47

R(18,19)	1.443	A(12,13,19)	112.82	D(1,6,26,25)	–29.94
R(18,20)	1.513	A(12,13,34)	108.98	D(1,6,26,27)	148.45
R(18,39)	1.095	A(14,13,19)	107.61	D(5,6,26,25)	149.25
R(20,21)	1.422	A(14,13,34)	113.11	D(5,6,26,27)	–32.35
R(20,40)	1.102	A(19,13,34)	107.88	D(2,7,8,9)	0.19
R(20,41)	1.098	A(13,14,15)	109.82	D(2,7,8,31)	–179.92
R(21,42)	0.961	A(13,14,16)	103.51	D(32,7,8,9)	–179.49
R(22,23)	1.403	A(13,14,35)	108.81	D(32,7,8,31)	0.40
R(22,27)	1.387	A(15,14,16)	114.40	D(7,8,9,10)	–0.02
R(22,28)	1.362	A(15,14,35)	111.15	D(7,8,9,33)	179.83
R(23,24)	1.389	A(16,14,35)	108.79	D(31,8,9,10)	–179.90
R(23,29)	1.375	A(14,15,36)	108.30	D(31,8,9,33)	–0.06
R(24,25)	1.392	A(14,16,17)	109.48	D(7,8,31,49)	–179.76
R(24,43)	1.086	A(14,16,18)	102.94	D(9,8,31,49)	0.13
R(25,26)	1.402	A(14,16,37)	108.00	D(8,9,10,3)	–0.24
R(25,44)	1.081	A(17,16,18)	115.82	D(8,9,10,30)	179.87
R(26,27)	1.404	A(17,16,37)	110.66	D(33,9,10,3)	179.91
R(27,45)	1.081	A(18,16,37)	109.44	D(33,9,10,30)	0.02
R(28,46)	0.966	A(16,17,38)	109.49	D(3,10,30,48)	–177.92
R(29,47)	0.962	A(16,18,19)	102.35	D(9,10,30,48)	1.96
R(30,48)	0.964	A(16,18,20)	113.41	D(5,12,13,14)	–163.92
R(31,49)	0.963	A(16,18,39)	111.11	D(5,12,13,19)	-46.07
		A(19,18,20)	109.34	D(5,12,13,34)	73.73
		A(19,18,39)	109.83	D(12,13,14,15)	–114.95
		A(20,18,39)	110.49	D(12,13,14,16)	122.49
		A(13,19,18)	108.88	D(12,13,14,35)	6.91
		A(18,20,21)	109.79	D(19,13,14,15)	123.81
		A(18,20,40)	108.23	D(19,13,14,16)	1.25
		A(18,20,41)	108.62	D(19,13,14,35)	–114.33
		A(21,20,40)	110.42	D(34,13,14,15)	4.76
		A(21,20,41)	111.36	D(34,13,14,16)	–117.80
		A(40,20,41)	108.33	D(34,13,14,35)	126.62
		A(20,21,42)	108.79	D(12,13,19,18)	–94.08
		A(23,22,27)	119.79	D(14,13,19,18)	23.13
		A(23,22,28)	120.62	D(34,13,19,18)	145.48
		A(27,22,28)	119.59	D(13,14,15,36)	167.12
		A(22,23,24)	120.17	D(16,14,15,36)	–77.02
		A(22,23,29)	115.32	D(35,14,15,36)	46.66
		A(24,23,29)	124.51	D(13,14,16,17)	–146.62
		A(23,24,25)	120.06	D(13,14,16,18)	–22.88
		A(23,24,43)	119.81	D(13,14,16,37)	92.82
		A(25,24,43)	120.13	D(15,14,16,17)	93.91
		A(24,25,26)	120.32	D(15,14,16,18)	–142.35
		A(24,25,44)	119.70	D(15,14,16,37)	–26.65
		A(26,25,44)	119.98	D(35,14,16,17)	–31.03

		A(6,26,25)	119.60	D(35,14,16,18)	92.71
		A(6,26,27)	121.19	D(35,14,16,37)	–151.59
		A(25,26,27)	119.19	D(14,16,17,38)	–172.90
		A(22,27,26)	120.46	D(18,16,17,38)	71.31
		A(22,27,45)	118.58	D(37,16,17,38)	–53.97
		A(26,27,45)	120.96	D(14,16,18,19)	36.37
		A(22,28,46)	108.58	D(14,16,18,20)	154.03
		A(23,29,47)	110.65	D(14,16,18,39)	–80.81
		A(10,30,48)	109.38	D(17,16,18,19)	155.80
		A(8,31,49)	110.10	D(17,16,18,20)	–86.54
				D(17,16,18,39)	38.62
				D(37,16,18,19)	–78.29
				D(37,16,18,20)	39.37
				D(37,16,18,39)	164.53
				D(16,18,19,13)	–37.56
				D(20,18,19,13)	–158.08
				D(39,18,19,13)	80.53
				D(16,18,20,21)	171.33
				D(16,18,20,40)	50.73
				D(16,18,20,41)	–66.68
				D(19,18,20,21)	–75.16
				D(19,18,20,40)	164.24
				D(19,18,20,41)	46.83
				D(39,18,20,21)	45.83
				D(39,18,20,40)	–74.77
				D(39,18,20,41)	167.82
				D(18,20,21,42)	169.43
				D(40,20,21,42)	–71.31
				D(41,20,21,42)	49.09
				D(27,22,23,24)	0.54
				D(27,22,23,29)	–179.73
				D(28,22,23,24)	–179.01
				D(28,22,23,29)	0.72
				D(23,22,27,26)	–0.39
				D(23,22,27,45)	179.97
				D(28,22,27,26)	179.17
				D(28,22,27,45)	–0.47
				D(23,22,28,46)	–0.89
				D(27,22,28,46)	179.56
				D(22,23,24,25)	0.01
				D(22,23,24,43)	179.92
				D(29,23,24,25)	–179.69
				D(29,23,24,43)	0.22
				D(22,23,29,47)	179.89
				D(24,23,29,47)	–0.40

				D(23,24,25,26)	–0.71
				D(23,24,25,44)	179.48
				D(43,24,25,26)	179.37
				D(43,24,25,44)	–0.43
				D(24,25,26,6)	179.29
				D(24,25,26,27)	0.86
				D(44,25,26,6)	–0.91
				D(44,25,26,27)	–179.33
				D(6,26,27,22)	–178.71
				D(6,26,27,45)	0.92
				D(25,26,27,22)	–0.31
				D(25,26,27,45)	179.32
*R: Bond length (Å), A: Bond angle (°), D: Dihedral angle (°).					

Table 4. Computed vibrational wavenumbers (cm^{-1}) of avicularin.

Mode number	Wavenumbers (computed)	Wavenumbers (scaled)	Assignments (%)
141	3848,73	3675.54	νOH (80.8)
140	3848,29	3675.12	νOH (81.6)
139	3841,40	3668.54	νOH (82.3)
138	3839,47	3666.70	νOH (82.6)
137	3836,57	3663.93	νOH (86)
136	3820,21	3648.30	νOH (87.7)
135	3795,73	3624.93	νOH (90.7)
134	3224,17	3079.08	νCH (73.6)
133	3219,35	3074.48	νCH (74.2)
132	3211,67	3067.14	νCH (76.4)
131	3155,68	3013.67	νCH (75.7)
130	3141,99	3000.60	νCH (74.6)
129	3085,30	2946.46	νCH (49.8)
128	3063,00	2925.16	ν_sCH (46.9)
127	3056,96	2919.40	ν_{as}CH (44.6)
126	3012,28	2876.73	ν_{as}CH (56.7)
125	2995,74	2860.93	ν_sCH (42.9)
124	2951,38	2818.56	ν_sCH (65.6)
123	1711,54	1655.06	νC=O (14.4)
122	1661,32	1606.50	νC=C (13.6) + νCC (13.2)
121	1654,13	1599.54	νC=C (11.3) + νCC (12.4)
120	1653,11	1598.56	νC=C (15.4) + νCC (11.9)
119	1632,78	1578.90	νC=C (16.2) + νCC (11.6)
118	1616,61	1563.26	νC=C (15.6) + νCC (13.2)
117	1539,26	1488.46	νCC (12.1) + νC=C (8.2)
116	1530,58	1480.07	νCC (14) + νC=C (8)

115	1495,87	1446.51	δHCH(12.6)
114	1494,38	1445.07	νC=C (8.9) + νCC (8.5)
113	1475,97	1427.26	νC=C (8.4) + νCC (7.9)
112	1466,74	1418.34	δCCH(17.8)
111	1451,00	1403.11	δOCH(8.1)
110	1417,82	1371.03	δOCH(8)
109	1408,07	1361.61	νC=C (3.9)
108	1395,16	1349.12	δOCH(9.3) + δOCH(8.5)
107	1383,73	1338.07	δOCH(9.8)
106	1376,68	1331.25	νCC (12.7) + νC=C (9.2)
105	1375,52	1330.13	νCC (15.5) + νC=C (12.6)
104	1355,25	1310.53	τHCCH (10.1)
103	1347,00	1302.55	τHCCH (15.3)
102	1338,42	1294.25	τHCCH (9.2)
101	1333,55	1289.54	δCCH(8.9)
100	1320,31	1276.74	δCCH(12.5)
99	1313,03	1269.70	δCCH(8.3)
98	1289,15	1246.61	δC=CH(12)
97	1287,20	1244.72	τHCCH (14.4) + δCCH(13.6)
96	1274,58	1232.52	δOCH(15.8) + τOCCH (13)
95	1269,73	1227.83	δC=CH(13.4)
94	1235,88	1195.10	δCOH(13.7)
93	1234,70	1193.95	δCOH(12.7)
92	1230,24	1189.65	δCOH(12.3) + δCCH(11.7)
91	1217,71	1177.52	δCCH(12.3)
90	1216,19	1176.06	δCCH(11.3)
89	1212,36	1172.35	δCOH(16.1) + δCCH(13.4)
88	1204,48	1164.73	δC=CH(11.8) + δCOH(9.4)
87	1192,11	1152.77	δCCH(8.6)
86	1173,95	1135.20	δC=CH(18.6) + δCOH(20.6)
85	1171,59	1132.93	δCCH(14.9)
84	1142,52	1104.82	δC=CH(10.7)
83	1122,62	1085.57	νCC (6.8)
82	1120,02	1083.05	δCCH(4.5)
81	1114,62	1077.84	δC=CH(5.6)
80	1104,43	1067.98	νCO (11.1)
79	1092,83	1056.77	νCO (9.4)
78	1081,33	1045.64	δCCH(7.4)
77	1077,01	1041.47	νCO (15)
76	1069,95	1034.64	νCO (12.1)
75	1042,83	1008.42	νCO (9.6)
74	1027,14	993.24	νCO (9.1)
73	1017,13	983.56	νCC (8.3)
72	997,96	965.03	νCC (8.8)
71	988,05	955.44	νCC (8.1)

70	957,15	925.56	νOC (5.8)
69	935,48	904.61	τHC=CH (15.3)
68	916,36	886.12	τCC=CH (16)
67	906,95	877.02	τCC=CH (6.2)
66	857,54	829.24	τHCOH (10.6)
65	847,26	819.30	δCC=C (6.3)
64	826,78	799.50	τHC=CO (13.4) + τOCCH (13.1) + τHC=CC (10.2) + τC=CCH (10.1)
63	815,39	788.48	τOCCH (5.1)
62	807,12	780.48	τOCCH (6.3)
61	793,63	767.44	νC=C (8.1)
60	779,71	753.98	τHC=CO (11.1) + τOCCH (10.7)
59	743,81	719.27	τOC=CC (3.9)
58	729,57	705.49	τCC=CC (5.7)
57	725,32	701.38	τCOCO (2.3)
56	710,99	687.53	τCC=CC (2.6)
55	694,20	671.29	τC=CCH (3.7)
54	674,91	652.64	τC=CC=C (8)
53	643,66	622.42	τHC=CC (3.8)
52	631,48	610.64	τHC=CC (4.2)
51	621,09	600.59	τHC=CC (2.7)
50	616,09	595.76	τHC=CC (5.2)
49	601,05	581.21	δCC=C (8.4)
48	594,43	574.82	δC=CO (2.8)
47	589,51	570.05	δCCH (2.7)
46	571,80	552.93	τCC=CC (4.4)
45	565,54	546.88	δC=CO (4.2)
44	560,57	542.07	τHCOH (5)
43	530,93	513.41	δC=CO (7.3)
42	504,55	487.90	τCCOH (2.8)
41	479,59	463.76	δCCO (5.7)
40	462,89	447.61	δCCO (2.8)
39	455,09	440.07	τC=COH (9.4)
38	434,91	420.56	τHCOH (3.2)
37	408,53	395.05	τCCOH (31.4) + τC=COH (29)
36	403,70	390.38	τCCOH (3.2)
35	396,32	383.24	τCCOH (5.3)
34	365,96	353.89	τCCOH (7.1)
33	362,59	350.62	τC=COH (11) + τC=COH (10.2)
32	355,64	343.90	τCCOH (12.9)
31	333,21	322.21	τCCOH (4.3)
30	326,78	316.00	τCCOH (14.5)

29	323,09	312.43	τCOC=C (2.6)
28	310,56	300.32	δC=CO (10.1)
27	304,25	294.21	τCCOH (19.5) + τC=COH (18.1)
26	293,67	283.98	τCCOH (16.7) + τC=COH (7.9)
25	273,81	264.77	τCCOH (16.9) + τHCOH (9.1)
24	264,17	255.46	τCCOH (27.7) + τHCOH (14)
23	257,84	249.33	τCCOH (8) + τC=COH (6.4)
22	245,29	237.20	τCCOH (29.4) + τHCOH (14.7)
21	235,91	228.13	τCCOH (24.3) + τHCOH (11.8)
20	231,14	223.51	τCCOH (16.4) + τHCOH (7.8)
19	218,90	211.68	τCCOH (12.7) + τC=COH (9.3)
18	212,57	205.56	τHCOH (19.8) + τCCOH (9.8)
17	209,94	203.02	τCCOH (18) + τC=COH (12.2) + τHCOH (10.4)
16	204,35	197.60	τCCOH (15) + τC=COH (13)
15	197,52	191.00	τCCOH (10.9) + τHCOH (8)
14	182,40	176.39	τHCOH (21.6) + τCCOH (11.2)
13	174,78	169.01	τHCOH (17.2) + τCCOH (9)
12	137,62	133.08	τCC=CO (6.2)
11	117,26	113.39	τHCOH (4.7)
10	102,47	99.09	τCCCH (10.1) + τOCCH (9.5)
9	90,51	87.52	τC=CC=O (3.2)
8	74,50	72.04	τCCOC (7.6)
7	66,29	64.10	τCCOC (3.8)
6	44,67	43.20	τOCCO (7.9)
5	40,18	38.85	τOCCO (7.7)
4	33,73	32.61	τCOCCa< mq (7.1)
3	28,53	27.59	τC=CCC (5.5) + τC=CC=C (5.4)
2	21,43	20.73	τC=CCC (4.3)
1	15,11	14.62	τOCCO (6.6)

4. Conclusions

Our research has highlighted the importance of the application of docking strategies based on selected flavonoids we retrieved from the ZINC database. We have presented how these flavonoids were oriented within the active site of the SARS–CoV–2 MPro. Our results suggested that a strong hydrogen bonding (1.65 Å) formed between the Gly–143 and we suggest that this can be attributed to an initial formation of a covalent bond. Most of our lead flavonoids showed H–bond interactions with Hie–41 and/or Cys–145, which were important residues for the catalytic activity of SARS–CoV–2 Mpro. At this point, we are aware that it is still not easy to make any direct conclusion because the nature and action mechanisms of both catalytic dyads and triads are still not clear. It should be noted that we did not use covalent bonding docking strategies, but our results can still be regarded as satisfactory.

Since molecular docking studies are almost the gold standard for screening new drugs and their targets, any type of candidate drug and determination of its interactions with SARS–CoV–2 Mpro is of importance. Based on our findings, the selected flavonoids could be promising inhibitors of SARS–CoV–2 MPro and they also need to be rapidly confirmed by experimental and clinical studies. We also suggest that the outcomes of this study can be led to design new and more potent drugs against fatal COVID–19 disease. It must be also considered that these findings solely might not be generalized to any other representative MPros of SARS–CoV–2 MPro. Taken together, our work clearly has some limitations, and the most important one is the lack of clinical applications that would confirm our results. Finally, our findings would seem to suggest that we have provided further evidence that flavonoids are potential inhibitors of SARS–CoV–2 MPro. Since the whole picture is still not complete, we believe that our results provide a stimulus for further research on docking of flavonoids to more Mpros and add to a growing body of literature on the way of understanding of mechanism of SARS–CoV–2.

References

[1] D.M. Knipe, P.M. Howley, "Fields Virology," Annals of Internal Medicine, 113 (1990) 258.

[2] "International Committee on Taxonomy of Viruses Virus taxonomy," (2018).

[3] "Center for Systems Science and Engineering at Johns Hopkins University," COVID-19 Dashboard., (2020).

[4] N. Zhu, D. Zhang, W. Wang, X. Li, B. Yang, J. Song, X. Zhao, B. Huang, W. Shi, R. Lu, P. Niu, F. Zhan, X. Ma, D. Wang, W. Xu, G. Wu, G.F. Gao, W. Tan, "A Novel Coronavirus from Patients with Pneumonia in China, 2019," New England Journal of Medicine, 382 (2020) 727–733.

[5] "Pfizer and BioNTech Announce Vaccine Candidate Against COVID-19 Achieved Success in First Interim Analysis from Phase 3 Study | Pfizer," (n.d.).

[6] "Moderna's COVID-19 Vaccine Candidate Meets its Primary Efficacy Endpoint in the First Interim Analysis of the Phase 3 COVE Study | Moderna, Inc.," (n.d.).

[7] "AZD1222 vaccine met primary efficacy endpoint in preventing COVID-19," (n.d.).

[8] "Oxford University breakthrough on global COVID-19 vaccine | Research | University of Oxford," (n.d.).

[9] T.T. Le, J.P. Cramer, R. Chen, S. Mayhew, "Evolution of the COVID-19 vaccine development landscape," Nature Reviews. Drug Discovery, 19 (2020) 667–668.

[10] "COVID19 Vaccine Tracker," (2021).

[11] E.P.K. Parker, M. Shrotri, B. Kampmann, "Keeping track of the SARS-CoV-2 vaccine pipeline," Nature Reviews Immunology, 20 (2020) 650.

[12] H. Chen, L.-S. Lee, G. Li, S.-W. Tsao, J.-F. Chiu, "Upregulation of glycolysis and oxidative phosphorylation in benzo[beta]pyrene and arsenic-induced rat lung epithelial transformed cells," Oncotarget, 7 (2016) 40674–40689.

[13] Y.N. Cao, L. Li, Z.M. Feng, S.Q. Wan, P.D. Huang, X.H. Sun, F. Wen, X.L. Huang, G. Ning, W.Q. Wang, "Comparative genetic analysis of the novel coronavirus (2019-nCoV/SARS-CoV-2) receptor ACE2 in different populations," Cell Discovery, 6 (2020).

[14] X. Liu, B. Zhang, Z. Jin, H. Yang, Z. Rao, "The crystal structure of COVID-19 main protease in complex with an inhibitor N3.," Protein Data Bank, (2020).

[15] Z. Jin, X. Du, Y. Xu, Y. Deng, M. Liu, Y. Zhao, B. Zhang, X. Li, L. Zhang, C. Peng, Y. Duan, J. Yu, L. Wang, K. Yang, F. Liu, R. Jiang, X. Yang, T.

You, X. Liu, X. Yang, F. Bai, H. Liu, X. Liu, L.W. Guddat, W. Xu, G. Xiao, C. Qin, Z. Shi, H. Jiang, Z. Rao, H. Yang, "Structure of Mpro from SARS-CoV-2 and discovery of its inhibitors," Nature, 582 (2020) 289–293.

[16] F.S. Wang, C. Zhang, "What to do next to control the 2019-nCoV epidemic?," The Lancet, 395 (2020) 391–393.

[17] B. Benarba, A. Pandiella, "Medicinal Plants as Sources of Active Molecules Against COVID-19," Frontiers in Pharmacology, 11 (2020) 1189.

[18] H.Z. Du, X.Y. Hou, Y.H. Miao, B.S. Huang, D.H. Liu, "Traditional Chinese Medicine: an effective treatment for 2019 novel coronavirus pneumonia (NCP)," Chinese Journal of Natural Medicines, 18 (2020) 206–210.

[19] K. Xu, H. Cai, Y. Shen, Q. Ni, Y. Chen, S. Hu, J. Li, H. Wang, L. Yu, H. Huang, Y. Qiu, G. Wei, Q. Fang, J. Zhou, J. Sheng, T. Liang, L. Li, "Management of corona virus disease-19 (COVID-19): the Zhejiang experience.," Zhejiang da xue xue bao. Yi xue ban = Journal of Zhejiang University. Medical sciences, 49 (2020) 147–157.

[20] H. Lu, "Drug treatment options for the 2019-new coronavirus (2019- nCoV)," 14 (2020) 69–71.

[21] Y.H. Jin, L. Cai, Z.S. Cheng, H. Cheng, T. Deng, Y.P. Fan, C. Fang, D. Huang, L.Q. Huang, Q. Huang, Y. Han, B. Hu, F. Hu, B.H. Li, Y.R. Li, K. Liang, L.K. Lin, L.S. Luo, J. Ma, L.L. Ma, Z.Y. Peng, Y.B. Pan, Z.Y. Pan, X.Q. Ren, H.M. Sun, Y. Wang, Y.Y. Wang, H. Weng, C.J. Wei, D.F. Wu, J. Xia, Y. Xiong, H.B. Xu, X.M. Yao, T.S. Ye, Y.F. Yuan, X.C. Zhang, Y.W. Zhang, Y.G. Zhang, H.M. Zhang, Y. Zhao, M.J. Zhao, H. Zi, X.T. Zeng, Y.Y. Wang, X.H. Wang, "A rapid advice guideline for the diagnosis and treatment of 2019 novel coronavirus (2019-nCoV) infected pneumonia (standard version)," Medical Journal of Chinese People's Liberation Army, 45 (2020) 1–20.

[22] H. De Groot, U. Rauen, "Tissue injury by reactive oxygen species and the protective effects of flavonoids," Fundamental and Clinical Pharmacology, 12 (1998) 249–255.

[23] A.R. Tapas, D.M. Sakarkar, R.B. Kakde, "Flavonoids as nutraceuticals," The Science of Flavonoids, 7 (2006) 213–238.

[24] G. Xu, J. Dou, L. Zhang, Q. Guo, C. Zhou, "Inhibitory effects of baicalein on the influenza virus in vivo is determined by baicalin in the serum," Biological and Pharmaceutical Bulletin, 33 (2010) 238–243.

[25] J. Dou, L. Chen, G. Xu, L. Zhang, H. Zhou, H. Wang, Z. Su, M. Ke, Q. Guo, C. Zhou, "Effects of baicalein on Sendai virus in vivo are linked to serum baicalin and its inhibition of hemagglutinin-neuraminidase," Archives of Virology, 156 (2011) 793–801.

[26] T.T.H. Nguyen, H.J. Woo, H.K. Kang, V.D. Nguyen, Y.M. Kim, D.W. Kim, S.A. Ahn, Y. Xia, D. Kim, "Flavonoid-mediated inhibition of SARS coronavirus 3C-like protease expressed in Pichia pastoris," Biotechnology Letters, 34 (2012) 831–838.

[27] S. Schwarz, D. Sauter, K. Wang, R. Zhang, B. Sun, A. Karioti, A.R. Bilia, T. Efferth, W. Schwarz, "Kaempferol derivatives as antiviral drugs against the 3a channel protein of coronavirus," Planta Medica, 80 (2014) 177–182.

[28] C.N. Chen, C.P.C. Lin, K.K. Huang, W.C. Chen, H.P. Hsieh, P.H. Liang, J.T.A. Hsu, "Inhibition of SARS-CoV 3C-like protease activity by theaflavin-3,3′- digallate (TF3)," Evidence-Based Complementary and Alternative Medicine, 2 (2005) 209–215.

[29] L. Chen, J. Li, C. Luo, H. Liu, W. Xu, G. Chen, O.W. Liew, W. Zhu, C.M. Puah, X. Shen, H. Jiang, "Binding interaction of quercetin-3-β-galactoside and its synthetic derivatives with SARS-CoV 3CLpro: Structure-activity relationship studies reveal salient pharmacophore

features," Bioorganic and Medicinal Chemistry, 14 (2006) 8295–8306.

[30] L. Yi, Z. Li, K. Yuan, X. Qu, J. Chen, G. Wang, H. Zhang, H. Luo, L. Zhu, P. Jiang, L. Chen, Y. Shen, M. Luo, G. Zuo, J. Hu, D. Duan, Y. Nie, X. Shi, W. Wang, Y. Han, T. Li, Y. Liu, M. Ding, H. Deng, X. Xu, "Small Molecules Blocking the Entry of Severe Acute Respiratory Syndrome Coronavirus into Host Cells," Journal of Virology, 78 (2004) 11334–11339.

[31] Y. Erdogdu, O. Unsalan, M. Tahir Gulluoglu, "FT-Raman, FT-IR spectral and DFT studies on 6, 8-dichloroflavone and 6,8-dibromoflavone," Journal of Raman Spectroscopy, 41 (2010) 820–828.

[32] Y. Erdoğdu, O. Ünsalan, M.T. Güllüoğlu, "Vibrational analysis of flavone," Turkish Journal of Physics, 33 (2009) 249–259.

[33] Y. Erdogdu, O. Unsalan, D. Sajan, M.T. Gulluoglu, "Structural conformations and vibrational spectral study of chloroflavone with density functional theoretical simulations," Spectrochimica Acta - Part A: Molecular and Biomolecular Spectroscopy, 76 (2010) 130–136.

[34] Y. Erdogdu, O. Unsalan, M. Amalanathan, I. Hubert Joe, "Infrared and Raman spectra, vibrational assignment, NBO analysis and DFT calculations of 6-aminoflavone," Journal of Molecular Structure, 980 (2010) 24–30.

[35] Y. Erdogdu, Ö. Dereli, D. Sajan, L. Joseph, O. Unsalan, M.T. Gulluoglu, "Vibrational (FT-IR and FT-Raman) spectral investigations of 7-aminoflavone with density functional theoretical simulations," Molecular Simulation, 38 (2012) 315–325.

[36] O. Unsalan, Y. Erdogdu, M.T. Gulluoglu, "FT-Raman and FT-IR spectral and quantum chemical studies on some flavonoid derivatives: Baicalein and Naringenin," Journal of Raman Spectroscopy, 40 (2009).

[37] S. Lalani, C.L. Poh, "Flavonoids as antiviral agents for enterovirus A71 (EV-A71)," Viruses, 12 (2020).

[38] S. Qian, W. Fan, P. Qian, D. Zhang, Y. Wei, H. Chen, X. Li, "Apigenin restricts FMDV infection and inhibits viral IRES driven translational activity," Viruses, 7 (2015) 1613–1626.

[39] J. Steinmann, J. Buer, T. Pietschmann, E. Steinmann, "Anti-infective properties of epigallocatechin-3-gallate (EGCG), a component of green tea," British Journal of Pharmacology, 168 (2013) 1059–1073.

[40] A. Chauhan, S. Kalra, "Identification of potent COVID-19 main protease (MPRO) inhibitors from flavonoids," (2020) 1–11.

[41] A.D. Mesecar, "A taxonomically-driven approach to development of potent, broad-spectrum inhibitors of coronavirus main protease including SARS-CoV-2 (COVID-19). To Be Published," (2020).

[42] K. Bolelli, T. Ertan-Bolelli, O. Unsalan, C. Altunayar-Unsalan, "Fenoterol and dobutamine as SARS-CoV-2 main protease inhibitors: A virtual screening study," Journal of Molecular Structure, 1228 (2021) 129449.

[43] H.T. Balaydin, S. Durdagi, D. Ekinci, M. Senturk, S. Goksu, A. Menzek, "Inhibition of human carbonic anhydrase isozymes I, II and VI with a series of bisphenol, methoxy and bromophenol compounds," Journal of Enzyme Inhibition and Medicinal Chemistry, 27 (2012) 467–475.

[44] S. Durdagi, "An Integrated Computational Approach for the Discovery of Ubiquitin Specific Protease 7 (USP7) Inhibitors as Potential Cancer Therapies," Biophysical Journal, 118 (2020) 47a-47a.

[45] G. Kayik, N.S. Tuzun, S. Durdagi, "In silico design of novel hERG-neutral sildenafil-like PDE5 inhibitors," Journal of Biomolecular Structure & Dynamics, 35 (2017) 2830–2852.

[46] S.S. Kulabas, F.C. Onder, Y.B. Yilmaz, A. Ozleyen, S. Durdagi, K. Sahin, M. Ay, T.B. Tumer, "In vitro and in silico studies of nitrobenzamide derivatives as potential anti-neuroinflammatory agents," Journal of Biomolecular Structure & Dynamics, (2019).

[47] S.A. Kulkarni, S.K. Nagarajan, V. Ramesh, V. Palaniyandi, S.P. Selvam, T. Madhavan, "Computational evaluation of major components from plant essential oils as potent inhibitors of SARS-CoV-2 spike protein," Journal of Molecular Structure, 1221 (2020) 128823.

[48] D.L. Ma, D.S.H. Chan, C.H. Leung, "Drug repositioning by structure-based virtual screening," Chemical Society Reviews, 42 (2013) 2130–2141.

[49] T. Mavromoustakos, S. Durdagi, C. Koukoulitsa, M. Simcic, M.G. Papadopoulos, M. Hodoscek, S.G. Grdadolnik, "Strategies in the Rational Drug Design," Current Medicinal Chemistry, 18 (2011) 2517–2530.

[50] S.B. Mirza, R.E. Salmas, M.Q. Fatmi, S. Durdagi, "Virtual screening of eighteen million compounds against dengue virus: Combined molecular docking and molecular dynamics simulations study," Journal of Molecular Graphics & Modelling, 66 (2016) 99–107.

[51] I.E. Orhan, F.S.S. Deniz, R.E. Salmas, S. Durdagi, F. Epifano, S. Genovese, S. Fiorito, "Combined molecular modeling and cholinesterase inhibition studies on some natural and semisynthetic O-alkylcoumarin derivatives," Bioorganic Chemistry, 84 (2019) 355–362.

[52] I.E. Orhan, D. Jedrejek, F.S. Senol, R.E. Salmas, S. Durdagi, I. Kowalska, L. Pecio, W. Oleszek, "Molecular modeling and in vitro approaches towards cholinesterase inhibitory effect of some natural xanthohumol, naringenin, and acyl phloroglucinol derivatives," Phytomedicine, 42 (2018) 25–33.

[53] E. Pitsillou, J. Liang, C. Karagiannis, K. Ververis, K.K. Darmawan, K. Ng, A. Hung, T.C. Karagiannis, "Interaction of small molecules with the SARS-CoV-2 main protease in silico and in vitro validation of potential lead compounds using an enzyme-linked immunosorbent assay," Computational Biology and Chemistry, 89 (2020) 1476–9271.

[54] K. Sahin, S. Durdagi, "Identifying new piperazine-based PARP1 inhibitors using text mining and integrated molecular modeling approaches," Journal of Biomolecular Structure & Dynamics, (2020).

[55] S. Durdagi, J.Q. Guo, J.P. Lees-Miller, S.Y. Noskov, H.J. Duff, "Structure-Guided Topographic Mapping and Mutagenesis to Elucidate Binding Sites for the Human Ether-a-Go-Go-Related Gene 1 Potassium Channel (KCNH2) Activator NS1643," Journal of Pharmacology and Experimental Therapeutics, 342 (2012) 441–452.

[56] R. Singh, A. Gautam, S. Chandel, A. Ghosh, D. Dey, S. Roy, V. Ravichandiran, D. Ghosh, R.E. Duval, R.J. Richardson, "molecules Protease Inhibitory Effect of Natural Polyphenolic Compounds on SARS-CoV-2: An In Silico Study," (2020).

[57] S. Durdagi, A. Kapou, T. Kourouli, T. Andreou, S.P. Nikas, V.R. Nahmias, D.P. Papahatjis, M.G. Papadopoulos, T. Mavromoustakos, "The application of 3D-QSAR studies for novel cannabinoid ligands substituted at the C1' position of the alkyl side chain on the structural requirements for binding to cannabinoid receptors CB1 and CB2," Journal of Medicinal Chemistry, 50 (2007) 2875–2885.

[58] S. Durdagi, C. Koukoulitsa, A. Kapou, T. Kourouli, T. Andreou, S.P. Nikas, V.R. Nahmias, D.P. Papahatjis, M.G. Papadopoulos, T. Mavromoustakos, "Testing the 3D QSAR/ComFA-CoMSIA results of flexible bioactive compounds with molecular docking studies," Drugs of the Future, 32 (2007) 79.

[59] S. Durdagi, T. Mavromoustakos, M.G. Papadopoulos, "3D QSAR

CoMFA/CoMSIA, molecular docking and molecular dynamics studies of fullerene-based HIV-1 PR inhibitors," Bioorganic & Medicinal Chemistry Letters, 18 (2008) 6283–6289.

[60] S. Durdagi, R.E. Salmas, M. Stein, M. Yurtsever, P. Seeman, "Binding Interactions of Dopamine and Apomorphine in D2High and D2Low States of Human Dopamine D2 Receptor Using Computational and Experimental Techniques," Acs Chemical Neuroscience, 7 (2016) 185–195.

[61] S. Durdagi, C.T. Supuran, T.A. Strom, N. Doostdar, M.K. Kumar, A.R. Barron, T. Mavromoustakos, M.G. Papadopoulos, "In Silico Drug Screening Approach for the Design of Magic Bullets: A Successful Example with Anti-HIV Fullerene Derivatized Amino Acids," Journal of Chemical Information and Modeling, 49 (2009) 1139–1143.

[62] J. Iqbal, M. Al-Rashida, S. Durdagi, V. Alterio, A. Di Fiore, "Recent Developments of Carbonic Anhydrase Inhibitors as Potential Drugs," Biomed Research International, (2015).

[63] G. Kayik, N.S. Tuzun, S. Durdagi, "Investigation of PDE5/PDE6 and PDE5/PDE11 selective potent tadalafil-like PDE5 inhibitors using combination of molecular modeling approaches, molecular fingerprint-based virtual screening protocols and structure-based pharmacophore development," Journal of Enzyme Inhibition and Medicinal Chemistry, 32 (2017) 311–330.

[64] S. Adem, V. Eyupoglu, I. Sarfraz, A. Rasul, M. Ali, "Identification of Potent COVID-19 Main Protease (Mpro) Inhibitors from Natural Polyphenols: An in Silico Strategy Unveils a Hope against CORONA," (2020).

[65] K.F. Azim, S.R. Ahmed, A. Banik, M.M.R. Khan, A. Deb, S.R. Somana, "Screening and druggability analysis of some plant metabolites against SARS-CoV-2: An integrative computational approach," Informatics in Medicine Unlocked, 20 (2020) 100367.

[66] P. Bellavite, A. Donzelli, "Hesperidin and SARS-CoV-2: New light on the healthy function of citrus fruits," Antioxidants, 9 (2020) 1–18.

[67] S.A. Cherrak, H. Merzouk, N. Mokhtari-Soulimane, "Potential bioactive glycosylated flavonoids as SARS-CoV-2 main protease inhibitors: A molecular docking and simulation studies," PLoS ONE, 15 (2020) 1–14.

[68] C.A. Ramos-Guzmán, J.J. Ruiz-Pernía, I. Tuñón, "Unraveling the SARS-CoV-2 Main Protease Mechanism Using Multiscale Methods," ACS Catalysis, 10 (2020) 12544–12554.

[69] M. Russo, S. Moccia, C. Spagnuolo, I. Tedesco, G.L. Russo, "Roles of flavonoids against coronavirus infection," Chemico-Biological Interactions, 328 (2020) 109211.

[70] Z. Xu, L. Yang, X. Zhang, Q. Zhang, Z. Yang, Y. Liu, S. Wei, W. Liu, "Discovery of Potential Flavonoid Inhibitors Against COVID-19 3CL Proteinase Based on Virtual Screening Strategy," Frontiers in Molecular Biosciences, 7 (2020) 1–8.

[71] F. Li, A.P. Michelson, R. Foraker, M. Zhan, P.R.O. Payne, "Computational analysis to repurpose drugs for COVID-19 based on transcriptional response of host cells to SARS-CoV-2," BMC Medical Informatics and Decision Making, 21 (2021) 1–13.

[72] R.A. Friesner, J.L. Banks, R.B. Murphy, T.A. Halgren, J.J. Klicic, D.T. Mainz, M.P. Repasky, E.H. Knoll, M. Shelley, J.K. Perry, D.E. Shaw, P. Francis, P.S. Shenkin, "Glide: A new approach for rapid, accurate docking and scoring. 1. Method and assessment of docking accuracy," Journal of Medicinal Chemistry, 47 (2004) 1739–1749.

[73] R.A. Friesner, R.B. Murphy, M.P. Repasky, L.L. Frye, J.R. Greenwood, T.A. Halgren, P.C. Sanschagrin, D.T. Mainz, "Extra precision glide: Docking and scoring incorporating a model of hydrophobic enclosure for protein-ligand complexes," Journal of

Medicinal Chemistry, 49 (2006) 6177–6196.

[74] A.D. Mesecar, “Structure of COVID-19 main protease bound to potent broad-spectrum non-covalent inhibitor X77,” (2020).

[75] T. Sterling, J.J. Irwin, “ZINC 15 – Ligand Discovery for Everyone,” Journal of Chemical Information and Modeling, 55 (2015) 2324–2337.

[76] “Schrödinger LLC. New York, USA:,” Schrodinger Inc., (2018).

[77] T.A. Halgren, R.B. Murphy, R.A. Friesner, H.S. Beard, L.L. Frye, W.T. Pollard, J.L. Banks, “Glide: A New Approach for Rapid, Accurate Docking and Scoring. 2. Enrichment Factors in Database Screening,” Journal of Medicinal Chemistry, 47 (2004) 1750–1759.

[78] H. Yang, M. Yang, Y. Ding, Y. Liu, Z. Lou, Z. Zhou, L. Sun, L. Mo, S. Ye, H. Pang, G.F. Gao, K. Anand, M. Bartlam, R. Hilgenfeld, Z. Rao, “The crystal structures of severe acute respiratory syndrome virus main protease and its complex with an inhibitor,” Proceedings of the National Academy of Sciences of the United States of America, 100 (2003) 13190–13195.

[79] Q. Zhao, S. Li, F. Xue, Y. Zou, C. Chen, M. Bartlam, Z. Rao, “Structure of the Main Protease from a Global Infectious Human Coronavirus, HCoV-HKU1,” Journal of Virology, 82 (2008) 8647–8655.

[80] F. Wang, C. Chen, W. Tan, K. Yang, H. Yang, “Structure of Main Protease from Human Coronavirus NL63: Insights for Wide Spectrum Anti-Coronavirus Drug Design,” Scientific Reports, 6 (2016) 1–12.

[81] R. Yoshino, N. Yasuo, M. Sekijima, “Identification of key interactions between SARS - CoV - 2 main protease and inhibitor drug candidates,” Scientific Reports, (2020) 1–8.

[82] H. Yang, W. Xie, X. Xue, K. Yang, J. Ma, W. Liang, Q. Zhao, Z. Zhou, D. Pei, J. Ziebuhr, R. Hilgenfeld, K.Y. Yuen, L. Wong, G. Gao, S. Chen, Z. Chen, D. Ma, M. Bartlam, Z. Rao, “Design of Wide-Spectrum Inhibitors Targeting Coronavirus Main Proteases,” Plos Biol., 3 (2005) e324–e324.

[83] L. Lecoq, C. Bougault, J.E. Hugonnet, C. Veckerlé, O. Pessey, M. Arthur, J.P. Simorre, “Dynamics induced by β-lactam antibiotics in the active site of Bacillus subtilis l,d-transpeptidase,” Structure, 20 (2012) 850–861.

[84] C.S. Ealand, E.E. Machowski, B.D. Kana, “β-lactam resistance: The role of low molecular weight penicillin binding proteins, β-lactamases and ld-transpeptidases in bacteria associated with respiratory tract infections,” IUBMB Life, 70 (2018) 855–868.

[85] Z. Jin, Y. Zhao, Y. Sun, B. Zhang, H. Wang, Y. Wu, Y. Zhu, C. Zhu, T. Hu, X. Du, Y. Duan, J. Yu, X. Yang, X. Yang, K. Yang, X. Liu, L.W. Guddat, G. Xiao, L. Zhang, H. Yang, Z. Rao, “Structural basis for the inhibition of SARS-CoV-2 main protease by antineoplastic drug carmofur,” Nature Structural and Molecular Biology, 27 (2020) 529–532.

[86] G.J. Lockbaum, A.C. Reyes, J.M. Lee, R. Tilvawala, E.A. Nalivaika, A. Ali, N.K. Yilmaz, P.R. Thompson, C.A. Schiffer, “Crystal structure of sars-cov-2 main protease in complex with the non-covalent inhibitor ml188,” Viruses, 13 (2021).

[87] S. Günther, P.Y. A Reinke, Y. Fernández-García, J. Lieske, T.J. Lane, H.M. Ginn, F.H. M Koua, C. Ehrt, W. Ewert, D. Oberthuer, O. Yefanov, S. Meier, K. Lorenzen, B. Krichel, J.-D. Kopicki, L. Gelisio, W. Brehm, I. Dunkel, B. Seychell, H. Gieseler, B. Norton-Baker, B. Escudero-Pérez, M. Domaracky, S. Saouane, A. Tolstikova, T.A. White, A. Hänle, M. Groessler, H. Fleckenstein, F. Trost, M. Galchenkova, Y. Gevorkov, C. Li, S. Awel, A. Peck, M. Barthelmess, F. Schlünzen, P. Lourdu Xavier, N. Werner, H. Andaleeb, N. Ullah, S. Falke, V. Srinivasan, B. Alves França, M. Schwinzer, H. Brognaro, C.

Rogers, D. Melo, J.J. Zaitseva-Doyle, J. Knoska, G.E. Peña-Murillo, A. Rahmani Mashhour, V. Hennicke, P. Fischer, J. Hakanpää, J. Meyer, P. Gribbon, B. Ellinger, M. Kuzikov, M. Wolf, A.R. Beccari, C. Uetrecht, R. Cox, A. Zaliani, T. Beck, M. Rarey, S. Günther, D. Turk, W. Hinrichs, H.N. Chapman, A.R. Pearson, C. Betzel, A. Meents, "X-ray screening identifies active site and allosteric inhibitors of SARS-CoV-2 main protease," Jonathan Pletzer-Zelgert, 18 (n.d.) 22.

[88] Y. Erdogdu, O. Unsalan, D. Sajan, M.T. Gulluoglu, "Structural conformations and vibrational spectral study of chloroflavone with density functional theoretical simulations," Spectrochimica Acta Part A: Molecular and Biomolecular Spectroscopy, 76 (2010) 130–136.

[89] O. Unsalan, Y. Erdogdu, M.T. Gulluoglu, "FT-Raman and FT-IR spectral and quantum chemical studies on some flavonoid derivatives: Baicalein and Naringenin," Journal of Raman Spectroscopy, 40 (2009) 562–570.

[90] Y. Erdogdu, O. Unsalan, M. Amalanathan, I. Hubert Joe, "Infrared and Raman spectra, vibrational assignment, NBO analysis and DFT calculations of 6-aminoflavone," Journal of Molecular Structure, 980 (2010) 24–30.

[91] Y. Erdogdu, O. Unsalan, M. Tahir Gulluoglu, "FT-Raman, FT-IR spectral and DFT studies on 6, 8-dichloroflavone and 6,8-dibromoflavone," Journal of Raman Spectroscopy, 41 (2010) 820–828.

[92] G. Varsanyi, Assignments for vibrational spectra of seven hundred benzene derivatives, Wiley, New York, 1974.

[93] J. Mohan, Organic Spectroscopy: Principles and Applications, Alpha Science Internatinoal, 2004.

[94] M. Heneczkowski, M. Kopacz, D. Nowak, A. Kuźniar, "Infrared spectrum analysis of some flavonoids," Acta Poloniae Pharmaceutica - Drug Research, 58 (2001) 415–420.

[95] J. Hanuza, P. Godlewska, E. Kucharska, M. Ptak, M. Kopacz, M. Mączka, K. Hermanowicz, L. Macalik, "Molecular structure and vibrational spectra of quercetin and quercetin-5'-sulfonic acid," Vibrational Spectroscopy, 88 (2017) 94–105.